Proc. of SPIE Vol. 2855, High Heat Flux Engineering III, ed. A M Khounsary (Nov 1996) Copyright SPIE

CVD Diamond for Optics Applications in High Heat Flux Environments

Claude A. Klein
c.a.k. analytics, inc.
9 Churchill Lane, Lexington, MA 02173

Abstract

Diamond has a cubic lattice structure and a very wide bandgap, which suggests that this material should exhibit excellent optical properties at wavelengths ranging from the far infrared to the near ultraviolet. Since diamond also exhibits unusually favorable properties in terms of mechanical strength, chemical stability, and thermal conductivity, there is considerable interest in using diamond for optics applications that involve adverse environmental conditions. The purpose of this paper is to provide an updated assessment of some of the issues that arise in connection with the use of chemically vapor-deposited (CVD) diamond for applications such as missile system windows or domes, and for designing components that must function in the high photon flux of high-power lasers. Specifically, since the flight velocities of future air-intercept missiles are projected to far exceed those of contemporary systems, this raises the issue of how to assess the capability of window/dome material candidates in an aero-thermal shock environment. In this context, it can be demonstrated that, compared to other candidate materials, diamond windows promise to deliver superior performances and should be able to meet any foreseeable requirement. Operation at high speeds, however, imposes limits on the tolerable window emittance to prevent "blinding" the seeker, and this issue leads to the conclusion that diamond is intrinsically unsuitable for operation in the 3- to 5-μm spectral band. Concerning high-energy lasers, note that operational systems always include an optical train consisting of mirrors and windows, which must be capable of transporting and directing the beam without seriously degrading the nominal performance of the laser In this regard, mirror-faceplate material candidates can be ranked on the basis of appropriate figures of merit, which demonstrate that diamond is of particular promise for high-heat-load applications that require efficient cooling. Finally, we emphasize that the power-handling capability of diamond laser windows must be examined in the light of potential limitations arising from thermal lensing effects induced by unfavorable refractive index characteristics; edge-cooled configurations may operate at CW beam-power levels of up to 0.5 MW, which is substantial but orders of magnitude below earlier predictions.

Keywords: diamond, domes, figures of merit, high-power lasers, infrared, mirror faceplates, missile systems, thermal lensing, thermal shock, windows

1. Introduction

Diamond has a cubic lattice structure and a very wide bandgap, which suggests that this material should exhibit excellent optical properties at wavelengths ranging from the far-infrared (IR) to the near-ultraviolet (UV). Since diamond also exhibits unusually favorable properties in terms of mechanical strength, chemical stability, and thermal conductivity, there is considerable interest in using diamond for optics applications that involve severe environmental conditions. The purpose of this paper is to provide an updated assessment of some of the issues that arise in connection with the use of chemically vapor-deposited (CVD) diamond for applications such as missile systems windows or domes and for designing components that must function in the high-photon-flux environment of high-power lasers. Diamond has many advantages and has been promoted as the "ultimate" optical material [1]; there are, however, limiting factors that must be taken into consideration. Multi-photon absorption [2] degrades the transmittance in the 2.5– to 7.5–μm wavelength range, which has important implications for contemplated military applications, and has not always been properly taken into account. Furthermore, while properties such as low thermal expansion and unsurpassed thermal conductivity point to exceptional power-handling capabilities, unfavorable refractive index characteristics (dn/dT) result in thermal lensing at power levels substantially below early speculations on the performance of diamond laser windows [3].

The property values I made use of in this evaluation of diamond for optics applications in high-heat-flux environments are listed in Table 1. These numbers originate from readily available sources and apply to CVD diamond keeping in mind that, to some extent, the properties depend on the quality of the deposit. In this connection, brief comments on the fracture strength, the elastic properties, and the infrared absorption are in order.

Table 1. Key Properties of CVD Diamond

Mass density:	$\rho = 3.52$ cm^{-3},	Ref. 4
Specific heat:	$C_p = 0.51$ g^{-1}K^{-1} at 293 K,	Ref. 4
Thermal expansion:	$\alpha = 0.8\times10^{-6}$ K^{-1} at 293 K,	Ref. 5
Thermal conductivity:	$k = 20$ Wcm^{-1}K^{-1} at 293 K,	Ref. 5
Young's modulus:	$E = 1140$ GPa,	Ref. 6
Poisson's ratio:	$\nu = 0.069$,	Ref. 6
Flexural strength:	$\sigma_f = 290$ MPa,	Ref. 7
Weibull modulus:	$m \simeq 2.5$,	Ref. 7
Refractive index:	$n = 2.41$ at 1 μm,	Ref. 8
Thermo-optic coefficient:	$dn/dT = 1\times10^{-5}$ K^{-1},	Ref. 8

- The measured strength of single-crystal diamond is of the order of 2.8 GPa [9], or roughly ten times the characteristic strength of free-standing CVD specimens [7], which demonstrates the overwhelming effect of lattice flaws in this material. Furthermore, the Weibull modulus was found to be quite low, thus reflecting a wide distribution of fracture probabilities that must be taken into account when CVD diamond components are subjected to thermo-mechanical loads.

- Since the elastic constants of single-crystal diamond are known with great accuracy [10], it is straightforward to derive exact numbers for both Young's modulus and Poisson's ratio of randomly orientated polycrystalline aggregates. In fact, measurements of the biaxial modulus, $E/(1-\nu)$, of randomly orientated as well as strongly textured CVD deposits [6] confirm that the elastic constants of high-quality CVD diamonds should be the same as those of natural type-IIa diamonds.

- Because CVD diamonds contain impurities and show evidence of lattice disorder, their spectral absorption features are not those of perfect 3C crystals. First-order (single-phonon) processes may occur, thus generating IR absorption in the 10–μm wavelength region [11], which strongly depends on the quality of the deposit.

The flight velocities of future-generation air-intercept missiles are projected to far exceed those of contemporary systems [12], which raises the issue of how to assess the capability of window/dome material candidates in an aero-thermal shock environment. In Sec. 2, I will demonstrate that, compared to other candidate materials, diamond windows promise to deliver superior performances in terms of thermo-structural capabilities and can easily meet present and foreseeable requirements. Operation at high speeds, however, imposes limits on the tolerable IR reemission to prevent "blinding" the detectors, and this issue requires special attention. Issues relating to diamond as a mirror or window material for high-power/high-energy laser systems will be addressed in Sec. 3. In this context, it is recalled that optical systems designed to project laser radiation to a distant target must operate close to the diffraction limit; in other words, the beam emerging from the exit aperture must be essentially aberration free, and we will examine how diamond performs in this regard. Finally, the conclusions are stated in Sec. 4, and the symbols are specified in the Appendix.

2. Missile Windows and Domes

In assessing the merits of CVD diamond as a window/dome material for high-speed missiles, it is essential to bear in mind that diamond is intrinsically unsuitable for operation in the 3– to 5–μm spectral band (Sec. 2.1). In terms of resistance to thermal shock, however, CVD diamond exhibits unmatched figures of merit (Sec. 2.2), which is attracting attention because presently available window/dome material candidates may not be able to handle the thermo-structural loads encountered on projected flight trajectories. This will be illustrated in Sec. 2.3 based on a "mid-altitude scenario" for air-to-air missiles that is representative of U.S. Air Force requirements [12].

2.1. The Reradiation Issue

Any IR window that becomes hot emits gray-body radiation over a wide spectral range, thus affecting the operation of the seeker system. It is generally recognized that saturation of the detectors by radiation from an aerodynamically heated window or dome is not a major problem, but the additional background noise may lower the performance of the system in terms of detection range as well as tracking ability [13]. If we assume that (a)

the seeker system has a wavelength-independent optical efficiency, (b) the sensor subsystem is detector-noise limited, and (c) the detectors all operate in a "blip" mode, the peak-signal to rms-noise ratio at the output terminals of the signal-processing unit can be expressed as follows:

$$SNR = \frac{H_{eff}}{NEI} . \tag{1}$$

The symbol H_{eff} refers to the net effective irradiance from the target, and NIE is the noise-equivalent irradiance,

$$NEI = (NEI)_o \sqrt{\frac{\phi}{\phi_o}} , \tag{2}$$

expressed in terms of the laboratory measured $(NEI)_o$ and the background photon-flux ratio ϕ/ϕ_o. The noise voltage is seen to be proportional to the square root of the number of incident background photons, which implies that the signal-to-noise ratio in the presence of window reradiation can be derived from the "dark system" SNR simply by writing

$$SNR = \frac{(SNR)_o}{\sqrt{\phi/\phi_o}} . \tag{3}$$

The ratio ϕ/ϕ_o thus determines the performance degradation and must be evaluated with care considering that the noise photons originate from three distinct sources: the detector surroundings, the background scene, and the hot window or dome.

If, for the sake of simplicity, we assume that the window emittance is independent of wavelength and temperature, in the spectral region of interest, the photon-flux ratio can be expressed in a relatively compact form [13],

$$\frac{\phi}{\phi_o} = \tau_o \frac{(1-\overline{E})Q(T_B) + (1/\tau_o - 1)Q(T_S) + \overline{E}Q(T_D)}{Q(T_o)} , \tag{4}$$

the symbol $Q(T)$ representing the effective quantum exitance at the temperature T, i.e.,

$$Q(T) = \int_{\lambda_1}^{\lambda_2} \frac{2\pi c \lambda^{-4}}{\exp\left[c_2/(\lambda T)\right] - 1} d\lambda , \tag{5}$$

where λ_1 and λ_2 are the cut-on/cut-off wavelengths of the sensor. Considering that the optical efficiency, that is, the transmittance of the optics including obscurations should be of the order of 50 % for state-of-the-art IR seekers, it becomes straightforward to describe the window-induced SNR degradation (in decibels) simply by plotting the function

$$10 \log \left[\frac{SNR}{(SNR)_o}\right] = -5 \log \left(\frac{\phi}{\phi_o}\right) \tag{6}$$

against the window temperature, for fixed values of the average emittance $\overline{E}$, as in Fig 1.[1] Since SNR degradations of more than 3 dB cannot be tolerated, it is seen that, if the system operates in the mid-IR, the average emittance should not exceed 0.2 %, which translates into absorption coefficients of less than 0.02 cm^{-1}, even for windows less than 1-mm thick.

[1]The background-scene temperature was set equal to 227 K (high-altitude scenario as in Ref. 12), which explains why the signal-to-noise ratio improves for domes that are not yet hot.

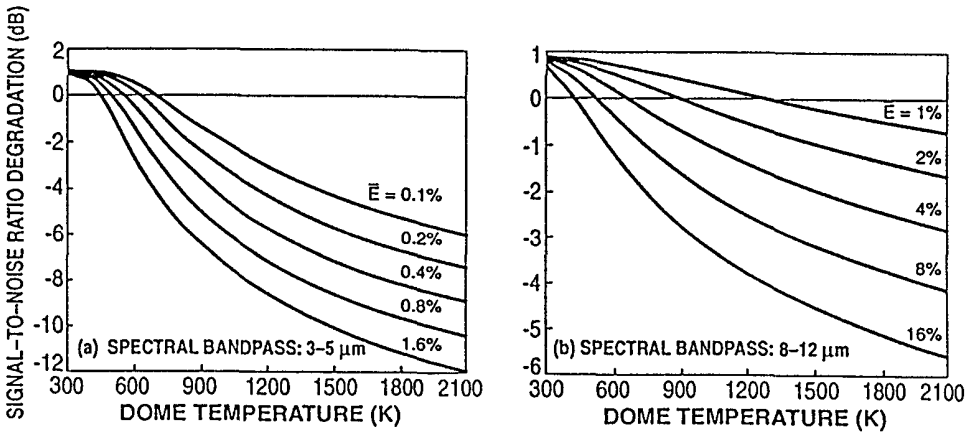

FIGURE 1. Signal-to-noise ratio (SNR) degradation of a hypothetical medium-wavelength/long-wavelength IR seeker as a function of the dome temperature for fixed average emittances. The temperature of the background scene was set equal to 227 K, while the seeker temperature was set at 300 K. The reference SNR is as measured in a laboratory setting.

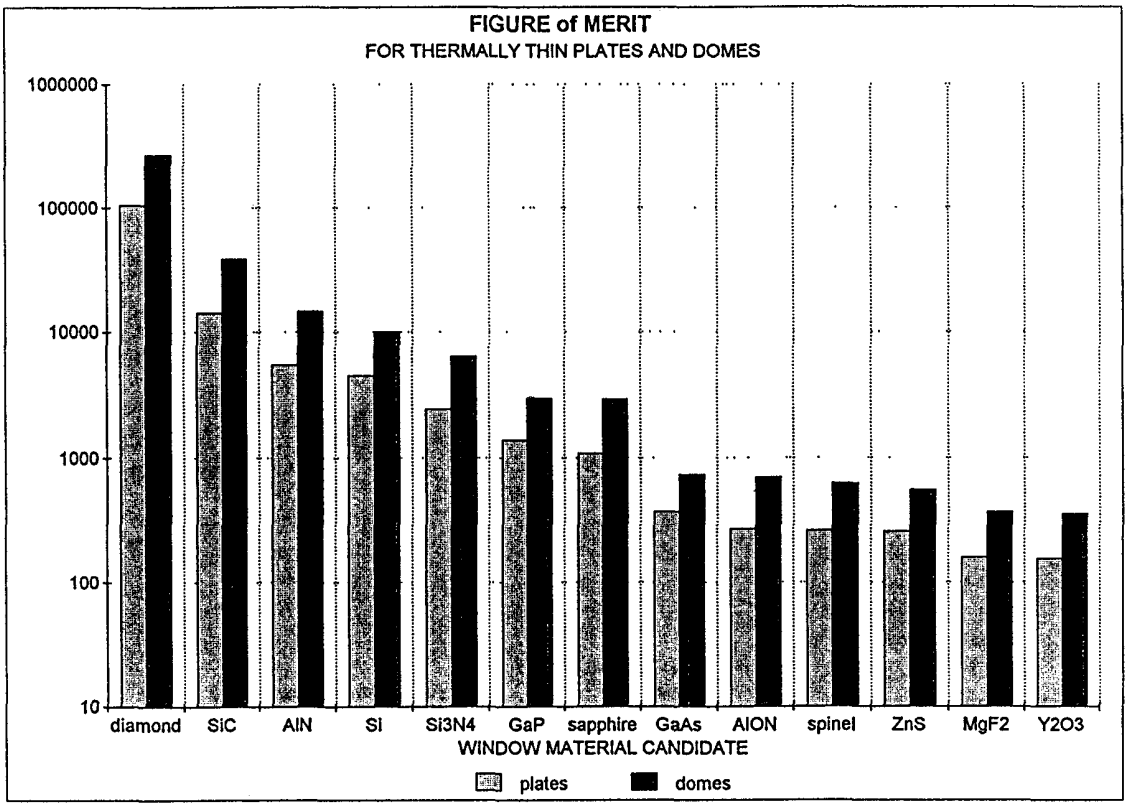

FIGURE 2. Figures of merit for thermal shock of missile-window material candidates in a thermally thin ($Bi < 1$) configuration. The units are as follows: $W(MPa)^{1/2}cm^{-1}$ for circular plates and $W(MPa)^{2/3}cm^{-1}$ for hemispherical shells. The relevant expressions are as given in Eq. (18), and all material properties are as measured at room temperature (a list of references is available upon request).

Such numbers are incompatible with well-established properties of diamond: The absorption coefficient peaks at frequencies where second-order processes dominate and reaches values of 12 cm^{-1} at about 5 μm [14], which leads to the conclusion that diamond is not an acceptable missile-window material for operation in the 3– to 5–μm spectral band. In the 8– to 12–μm spectral band, on the contrary, the system may function even if the window emittance exceeds 10 %, which means absorption coefficients that are easily achievable with CVD diamond [11], especially since single-phonon absorptions do not exhibit much temperature dependence [15].

2.2. FoM for Thermal Shock

The sudden exposure to a supersonic flight environment subjects a missile window or dome to intense convective heat loads stemming from the rise in temperature of the boundary layer, that is, the air in immediate contact with the outer surface. The thermal response of the window then results in temperature gradients through the thickness, which in turn generates transient stresses that may exceed the tensile strength of the material, thus causing thermal shock induced fracture. To describe this shock, I rely on the following expression for the peak stress [16]:

$$\sigma_p = \frac{1}{TSF} \cdot \frac{\alpha E}{1-\nu} \cdot \Delta T_p \ , \tag{7}$$

where TSF represents the thermal stress factor, which depends on a number of factors,[2] and ΔT_p is the peak temperature differential across the wall. In a previous paper [17], it was shown that the initial transient temperature distribution can be modeled quite effectively in the framework of the "lumped parameter approximation," which has the advantage of providing some insight into the physical mechanisms that govern the thermal stress. In the transient phase, ΔT is a strong function of time and depends critically on the heat-transport process as characterized by the Biot number,

$$Bi \equiv hL/k \ , \tag{8}$$

where h denotes the heat-transfer coefficient, L is the window/dome thickness, and k its thermal conductivity; I will refer to $Bi > 1$ situations as "thermally thick" and to $Bi < 1$ situations as "thermally thin." In this framework, the peak temperature differential can be approximated in a very simple manner:

$$\Delta T_p \simeq \begin{cases} Q/h & \text{if} \quad Bi > 1 \\ Q(L/k) & \text{if} \quad Bi < 1 \end{cases} \ , \tag{9}$$

where the symbol Q refers to the flight-induced heat flux.

Assume now that the failure stress relates to the nominal strength of the window/dome material through the fracture statistical factor FSF, i.e.,

$$(\sigma_p)_{\text{lim}} = \frac{\sigma_f}{FSF} \ . \tag{10}$$

[2]For example, $TSF = 2$ for a clamped circular plate —or a complete sphere—if there is a linear temperature variation across the thickness and both surfaces are free to expand.

The allowable heat flux then obeys the following relations:

$$Q_{\text{lim}} \simeq \begin{cases} \frac{TSF}{FSF} \cdot \frac{\sigma_f (1-\nu)}{\alpha E} \cdot h & \text{if} \quad Bi > 1 \\ \frac{TSF}{FSF} \cdot \frac{\sigma_f (1-\nu)}{\alpha E} \cdot \frac{k}{L} & \text{if} \quad Bi < 1 \end{cases} , \tag{11}$$

which immediately suggests to use figures of merit (FoM) for rating the ability of window/dome materials to withstand thermal shocks. In a thermally thick regime the figure of merit derives directly from Eq. (11),

$$(FoM)_{Bi>1} = \frac{\sigma_f (1-\nu)}{\alpha E} , \tag{12}$$

and is seen to replicate the Hasselman "parameter" for strong shocks [18].

Under thermally thin conditions, however, the thickness L plays an essential role in the sense that the thermal shock resistance will be enhanced by making the window or dome as thin as possible [see Eq. (11)]. For this reason, and for the purpose of evaluating the ultimate performance of a window material candidate, it should be appropriate to write

$$Q^*_{\text{lim}} \simeq \frac{TSF}{FSF} \cdot \frac{\sigma_f (1-\nu) k}{\alpha E} \cdot \frac{1}{L_{\text{min}}} \tag{13}$$

and insert suitable expressions for the acceptable minimum window thickness. For instance, since the maximum tensile stress occurring in a clamped circular plate of diameter D subjected to a uniform pressure load Δp is [16]

$$\sigma_{\text{max}} = \frac{3/16}{(L/D)^2} \Delta p , \tag{14}$$

the window must have an aspect ratio larger or equal to

$$\frac{L_{\text{min}}}{D} = 0.433 \sqrt{DSF} \sqrt{\frac{\Delta p}{\sigma_f}} \tag{15}$$

if DSF represents the design safety factor ($2 \leq DSF \leq 4$ depending on the Weibull modulus). Similarly, the maximum bending stress of a freely supported truncated hemispherical shell of radius R depends solely on the relative wall thickness and can be approximated as follows [17]:

$$\sigma_{\text{max}} \simeq \frac{0.581}{(L/R)^{3/2}} \Delta p , \tag{16}$$

which leads to a required aspect ratio

$$\frac{L_{\text{min}}}{R} \simeq 0.696 \, (DSF)^{2/3} \left(\frac{\Delta p}{\sigma_f} \right)^{2/3} . \tag{17}$$

Returning now to Eq. (13), it is seen that the allowable heat flux in a thermally thin environment depends on both the geometry and the attachment, which translates into figures of merit

$$(FoM)_{Bi<1} = \begin{cases} \dfrac{\sigma_f^{3/2} (1-\nu) k}{\alpha E} & \text{for} \quad \text{clamped plates} \\ \dfrac{\sigma_f^{5/3} (1-\nu) k}{\alpha E} & \text{for} \quad \text{free shells} \end{cases} \tag{18}$$

for characterizing the ability of missile window materials to withstand thermal shocks. Evidently, the frequently used Hasselman "parameter" for mild shocks [18], $R' = \sigma_f (1 - \nu)k/(\alpha E)$, does not provide a conceptually sound formula for assessing the intrinsic capability of candidate materials in the thermally thin environment typical of air-intercept missiles.

The bar chart displayed in Fig. 2 depicts the results of evaluating $(FoM)_{Bi<1}$ for a number a window material candidates presently under consideration; note that the units are $\mathrm{W(MPa)^{1/2}cm^{-1}}$ for thin plates and $\mathrm{W(MPa)^{3/2}cm^{-1}}$ for hemispherical shells. The figure of merit involves five key material properties—elastic modulus E, expansion coefficient α, flexural strength σ_f, Poisson's ratio ν, thermal conductivity k—and care must be exercised in selecting proper numerical values; for consistency the property values I used all refer to room temperature. As evidenced in Fig. 2, the ranking is the same for plates as for shells, thus emphasizing the clearly superior thermal shock performance of CVD diamond in a thermally thin situation.

2.3. A Case Study

Because of the thermal expansion mismatch at the interface of an IR dome and its support ring, it is generally accepted [19] that a "floating" attachment scheme that decouples the dome from the missile body must be implemented to ensure that the attachment does not inject additional stresses that may impair the thermal shock performance. Furthermore, for dome configurations and flight regimes currently under consideration, the Biot number is always representative of a thermally thin environment [17], and based on evidence presented elsewhere [20], the ratio TSF/FSF should be set equal to two. In this light, it is seen that the allowable heat flux on a thickness optimized missile dome is best expressed as follows:

$$Q^*_{\mathrm{lim}} \simeq 2\frac{\sigma_f (1-\nu)k}{\alpha E} \cdot \frac{1}{L_{\mathrm{min}}} , \tag{19}$$

which leads to

$$Q^*_{\mathrm{lim}} \simeq \frac{1.14\,(FoM)_{Bi<1}}{R(\Delta p)^{2/3}} \tag{20}$$

since the required thickness [see Eq. (17)] is

$$L_{\mathrm{min}} = 1.75R\left(\frac{\Delta p}{\sigma_f}\right)^{2/3} \tag{21}$$

if the design safety factor is set equal to four.

Equation (20) emphasizes that, given the radius of the dome, it is the figure of merit $(FoM)_{Bi<1}$ that controls the performance in a specified aero environment. To illustrate, consider a medium-altitude scenario as postulated in Ref. 12, i.e.,

$$Z = 3 \text{ km (10,000 ft)}, \qquad M_\infty = 4, \qquad R = 3.81 \text{ cm (1.5 in)},$$

which is very stressing since the pressure differential [21],

$$\Delta p = p_\infty \left\{ \frac{\left[\left(\frac{\gamma+1}{2}\right) M_\infty^2\right]^{\frac{\gamma}{\gamma-1}}}{\left[\frac{2\gamma}{\gamma+1} M_\infty^2 - \frac{\gamma-1}{\gamma+1}\right]^{\frac{1}{\gamma-1}}} - 1 \right\} , \tag{22}$$

amounts to 203 psi (1.40 MPa). Returning now to Eq. (20), and on inserting the figure of merit for diamond domes as given in Fig. 2, we find that the allowable heat flux is of the order of 50 kW/cm^2.

Under laminar flow conditions, the boundary-layer temperature and the heat-transfer coefficient both reach maximum values at the stagnation point, which implies that, in the lumped parameter approximation, the critical heat flux is

$$Q_{st} = h_{st}\,(T_{st} - T_{iw}) \ , \tag{23}$$

where T_{iw} refers to the wall temperature at the onset of the shock. The heat-transfer coefficient can be expressed in a manner such as [22]

$$h_{st} \simeq 1.20\, c_p \sqrt{\frac{\rho_\infty \mu_\infty a_\infty}{R}}\, M_\infty \left(1 + \frac{\gamma - 1}{2} M_\infty^2\right)^{0.1} \ , \tag{24}$$

which yields $h_{st} \simeq 0.21$ Wcm^{-2}K^{-1} for a 1.5-in dome on a medium-altitude trajectory. Since the stagnation temperature,

$$T_{st} = T_\infty \left[1 + \left(\frac{\gamma - 1}{2}\right) M_\infty^2\right] \ , \tag{25}$$

is equal to 1121 K at Mach 4 and an altitude of 3 km (U.S. Standard Atmosphere), it follows that the heat flux Q_{st} does not exceed 160 W/cm^2 if the initial dome temperature reflects an external-carry launch at Mach 1.5 as postulated in Ref. 12. Since the allowable flux is at least three hundred times larger, diamond domes easily survive such shocks,[3] but since the recovery temperature approaches 850 °C, problems may arise as the oxidation rate becomes significant [9]; durable coatings will be required to provide adequate protection. Finally, I may point out that, according to Eq. (21), a 1.5–in radius diamond dome must be about 2 mm thick to withstand the aerodynamic pressure on a medium-altitude trajectory, which means $Bi \simeq 0.002$ and "explains" the outstanding resistance to thermal shock.

3. Laser Mirrors and Windows

High-energy laser (HEL) systems include an optical train consisting of mirrors and windows, which must be capable of transporting and directing the beam without seriously degrading the nominal performance of the laser. Available experience shows that catastrophic failure modes associated with thermally generated stresses or laser-induced damage are not a major threat at beam-power levels of current interest; the performance of the system as measured in terms of achievable target irradiances usually degrades because of "thermal lensing," that is, the process of beam defocusing and beam distortion caused

[3] In this connection, it is interesting that sapphire, the currently prevalent IR dome material for demanding applications [23], has a figure of merit $(FoM)_{Bi<1}$ of about 2 kW(MPa)$^{3/2}$cm^{-1}, which means $Q^*_{\rm lim} \simeq 475$ W/cm^2 for the situation of interest here. In a fully laminar boundary-layer regime, sapphire domes will survive, but this may not be true if a transition to turbulent flow occurs, which enhances the heat flux by a factor of two or three [24].

by thermally generated phase aberrations [25]. In this chapter, I will first address this issue (Sec. 3.1), then derive figures of merit for mirror-faceplate materials to demonstrate the superior capability of CVD diamond (Sec. 3.2), and look at an edge-cooled diamond window to assess the power-handling capability in the light of limitations imposed by refractive index characteristics (Sec. 3.3).

3.1. The Thermal Lensing Issue

Laser systems components such as mirrors and windows always absorb a fraction of the incident radiation, which gives rise to thermal loadings that can lead to phase distortions and, ultimately, to stress-induced fracture. At high-average-power levels, these components must be cooled in order to avoid catastrophic failure; in conjunction with non-uniform incident power distributions this causes temperature gradients across the aperture and, by the same token, creates optical distortions. In most instances, beam-induced distortions represent the primary failure mode in the sense that they impose strict limits on the total power, or the total energy, that can be successfully handled by the system.

For this reason, the performance of candidate materials for mirror faceplates as well as laser windows must be assessd on the basis of their ability to minimize wavefront distortions induced by beam-generated thermal loadings [26]. If the distortions are axially symmetric and do not involve birefringence effects, the far-field intensity derives from the Huygens-Fresnel integral [27] and is given by the expression

$$I_{GF}(t) = \left(\frac{2\pi/\lambda}{Z_o}\right)^2 \left| \int_0^{D/2} \sqrt{I(r)} \exp\left[i\delta\phi\,(r,t)\right] r\,dr \right|^2 , \tag{26}$$

in a cylindrical geometry. The phase-aberration function $\delta\phi\,(r,t)$ maps the cumulative aberrations impressed on the beam while propagating through the system and relates to the optical path difference (OPD) simply through the propagation constant $2\pi/\lambda$. In the absence of aberrations, that is, at the onset of thermal loadings (t=0), the beam intensity at the Gaussian focus is

$$I_{GF}(0) = BPF \frac{\pi\,(D/2)^2\,P}{(\lambda Z_o)^2} \tag{27}$$

if BPF denotes the beam profile factor that accounts for the reduction in far-field intensity caused by non-uniform beam intensities. As near-field phase aberrations emerge, the degradation in focal intensity obeys a Strehl-type equation [28],

$$I_{GF}(t) = I_{GF}(0) \times SR \tag{28}$$

with

$$SR = 1 - \mathrm{var}[\delta\phi] = 1 - (2\pi/\lambda)^2\,\mathrm{var}[OPD] , \tag{29}$$

which says that the optical train will remain nearly diffraction limited as long as the variance of the OPD does not exceed a specified limit; note that the variance is defined as follows:

$$\mathrm{var}[X] = \left\langle X^2 \right\rangle - \langle X \rangle^2 , \tag{30}$$

the brackets symbolizing amplitude-weighted averages over the entire aperture:

$$\langle X^n \rangle = \frac{\int_0^1 X^n \sqrt{I(\rho)}\rho\,d\rho}{\int_0^1 \sqrt{I(\rho)}\rho\,d\rho} . \tag{31}$$

Equation (29) provides an effective tool for evaluating the loss in focal irradiance caused by beam-induced aberrations, and I will rely on suitable expressions for the magnitude of $\sqrt{\text{var}[OPD]}$ to derive figures of merit for diamond mirror faceplates and estimate the power-handling capability of diamond laser windows.

3.2. Mirror-Faceplate Material Evaluation

Thermally induced mirror surface deformations resulting from spatial variations in beam intensity generate wavefront distortions that impact the system's performance through the RMSsed OPD, which is

$$\sqrt{\text{var}[OPD]} = 2\sqrt{\text{var}[\delta l]} \tag{32}$$

at normal incidence, if δl refers to the out-of-plane growth of the mirror front surface.[4] If the back of the mirror faceplate can be maintained in its original plane ($z = 0$), this growth amounts to

$$\delta l = \int_0^l \epsilon_z(z)\, dz \ , \tag{33}$$

where ϵ_z is the position-dependent strain for axial expansion including stress related contributions in accord with Hooke's law [29]. Thermally induced strains are difficult to evaluate in a situation as applies here, but for thin mirror faceplates ($l/D \ll 1$), plane-stress theory indicates that the relevant expression reduces to

$$\epsilon_z(z) = \alpha(1+\nu)\delta T - 2\alpha\nu \int_0^1 \delta T\, \rho' d\rho' \tag{34}$$

in the case of axisymmetric loadings of elastically isotropic disks.

Assume now that a short pulse of laser light impinges on the mirror front surface. The deposited local beam fluence, $A_M I(\rho)t$, generates a temperature distribution $\delta T(\rho, z, t)$ that obeys the integral equation

$$A_M I\,(\rho)\, t = C_p' \int_0^l \delta T(\rho, z, t) dz \ , \tag{35}$$

where A_M is the mirror absorbance and C_p' is the heat capacity (specific heat per unit volume) of the faceplate. Returning now to Eq. (33), it is seen that, prior to the onset of significant radial diffusion or heat loss across the back surface, the front-surface deformation can be expressed as follows:

$$\delta l(\rho) = \alpha(1+\nu) A_M I(\rho) t\, / C_p' + \rho\text{-independent terms} \ , \tag{36}$$

which yields

$$(FoM)_{sp} = \frac{C_p'}{|\alpha|\,(1+\nu)} \tag{37}$$

[4] Mirror "bowing" can be compensated by refocusing and, therefore, can be ignored in the context of assessing the thermal lensing performance of HEL reflectors.

for the single-pulse figure of merit of mirror materials,[5] keeping in mind that ρ-independent terms do not contribute to the variance.

At high-average-power levels, the deposited beam energy must be removed by means of a heat exchanger, and Fig. 3 illustrates the design concept currently implemented for manufacturing actively cooled high-power laser-light reflectors [30]. In thermal equilibrium—or steady-state situation—, and on assuming that the thickness of the faceplate is small relative to the scale of spatial variations in beam intensity, there is a constant flow of heat, $A_M I$, across the back surface, which gives rise to a linear temperature gradient through the mirror faceplate (see Fig. 3):

$$T(z) - T(0) = (A_M I\,/k)z\ . \tag{38}$$

Since the local temperature at the back is

$$T(0) = A_M I\,/h \tag{39}$$

if measured against the coolant, it follows that CW (or quasi-CW) laser irradiation results in a temperature profile

$$\delta T(z) = A_M I \left(\frac{1}{h} + \frac{z}{k}\right)\ . \tag{40}$$

At this point, a simple integration yields

$$\delta l = \alpha(1+\nu)\left(\frac{l}{h} + \frac{l^2}{2k}\right) A_M I + \rho\text{-independent terms}, \tag{41}$$

and if we introduce the Biot number $Bi = lh/k$ to characterize the efficiency of the heat-exchange process, it is seen that the RMSsed surface deformation can be expressed in a manner such as

$$\sqrt{\text{var}[\delta l]} = \frac{|\alpha|\,(1+\nu)l}{h}\left(1 + \frac{Bi}{2}\right) A_M \sqrt{\text{var}[I\,]} \tag{42}$$

that best specifies how the performance of the mirror assembly depends on material properties and design features. It is immediately apparent that the faceplate should be as thin as possible but not thinner than required to minimize coolant-induced pressure ripples, which points to the modulus of elasticity E as an important faceplate-material property to consider [31]; in effect, since the deflection is essentially a linear function of the inverse flexural rigidity [16], the minimum thickness should be proportional to $1/\sqrt[3]{E'}$ if E' is set equal to $E/(1-\nu^2)$. The figures of merit that emerge from Eq. (42) are then as follows:

$$(FoM)_{ss} = \begin{cases} \dfrac{\sqrt[3]{E'}}{|\alpha|\,(1+\nu)} & \text{if} \quad Bi \ll 1 \\ \dfrac{\sqrt[3]{E'^2 k}}{|\alpha|\,(1+\nu)} & \text{if} \quad Bi \gg 1\ , \end{cases} \tag{43}$$

thus emphasizing that the cooling efficiency is another factor to take into account.

[5] Since multi-layer coatings are required to enhance the reflectivity, it is the coating that determines the magnitude of the mirror absorbance A_M.

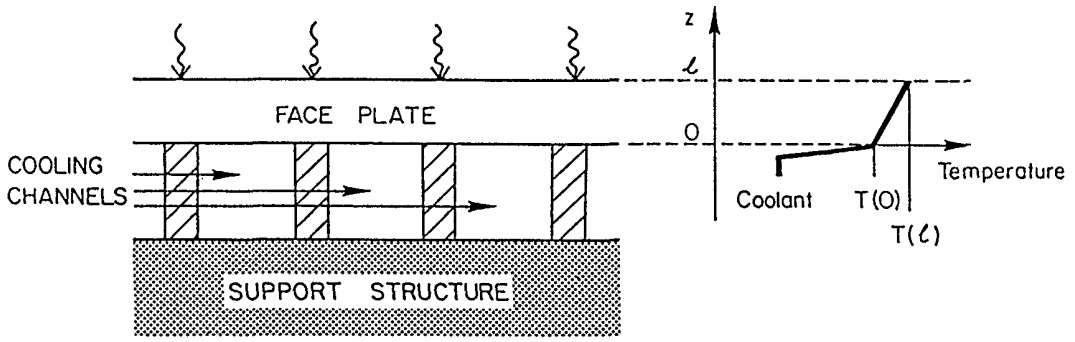

FIGURE 3. Schematic representation of a high-energy-laser mirror assembly. The backside of the faceplate interfaces with the coolant fluid to ensure adequate heat transfer; the cooling channels are mounted on a support structure designed to provide a stable, highly rigid base. The axial temperature profile on the right refers to a steady-state situation and assumes minimal radial heat diffusion.

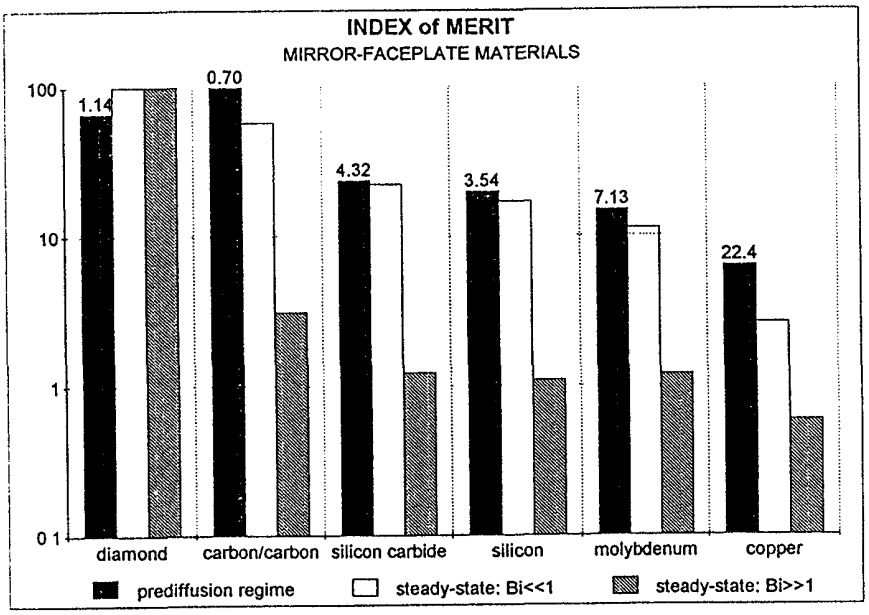

FIGURE 4. Index of merit for thermal lensing of key mirror-faceplate materials. An index of 100 is assigned to the "best" candidate for each of the three operational regimes (Bi is the Biot number). The data labels are the values of the "thermal distortion coefficient," $|\alpha|(1+\nu)$, in units of $10^{-6}\mathrm{K}^{-1}$ and demonstrate that the expansion coefficient essentially controls the performance.

Figure 4 displays the ranking of HEL mirror material candidates [30], including diamond, based on normalized figures of merit, or indices of merit $IoM \equiv 100 \times FoM/FoM_{\max}$, where $FoM_{\max}$ is the figure of merit of the candidate material best suited for the contemplated application; the property data I used are those listed in Ref. 32 and refer to temperatures of 350 K. This procedure demonstrates that mirror materials can be ranked with regard to overall performance in the sense that if a material is superior in one application it is also superior in the others, which evidently confirms that the thermal expansion is the determining factor. The two carbon materials, cubic carbon (diamond) and carbon/carbon composites, are both seen to be outstanding candidates, diamond exhibiting particular promise for high-heat-load optics applications that require efficient cooling, which has already attracted attention in the synchrotron community.

3.3. Edge-Cooled Diamond Windows

In diamond, infrared absorption occurs primarily within the two- and three-phonon spectral regions, that is, in a wavenumber range that extends from one to three times the Raman frequency (1333 to 3999 cm^{-1}); at frequencies above 4000 cm^{-1}, the intrinsic absorption of diamond should be very low and remain low throughout the near-IR and the visible. At wavelengths of, say 1 μm, it is reasonable to expect that nearly perfect synthetic diamonds will have absorption coefficients of less that 1×10^{-4} cm^{-1}. In conjunction with the exceptional thermal conductivity, this makes diamond an obvious candidate for high-power laser-window applications, which calls for examining the power-handling capability of an edge-cooled configuration [33] in the light of potential limitations arising from thermal lensing effects.

Window-induced wavefront distortions involve fairly complex phenomena because the phaseshifts reflect not only position-dependent variations of the window thickness but also position- and polarization-dependent variations of the refractive index [34]. Diamond has a positive thermo-optic coefficient dn/dT (see Table 1), which dominates the lensing process in the sense that the effective optical distortion coefficient reduces to

$$\chi = \frac{dn}{dT} + (n-1)\alpha(1+\nu) \tag{44}$$

and does not require attention to photo-elastic effects. Since the variance of the OPD is equal to $(\chi L)^2 \mathrm{var}[\delta T]$, where δT denotes the beam-induced temperature increment averaged over the window thickness, the degradation in focal intensity caused by thermal lensing originates from

$$\sqrt{\mathrm{var}[OPD]} = \frac{\chi A_W P}{k}\sqrt{\mathrm{var}[\delta T^*]} \tag{45}$$

upon introducing the reduced temperature δT^* [35].[6] For edge-cooled windows, the steady-state temperature increment δT^* is a solution of the heat-flow equation that satisfies the boundary condition $\delta T(1) = 0$, i.e.,

$$\delta T^*(\rho) = \frac{1}{f_o}\int_\rho^1 \frac{d\rho'}{\rho'}\int_0^{\rho'} f(\rho'')\rho''d\rho'' \ , \tag{46}$$

[6]The radial temperature profile of cooled laser windows is best described in terms of the dimensionless temperature δT^* defined as follows: $\delta T = (\beta P/k)\delta T^*$, where β is the absorption coefficient ($\beta = A_W/L$), P is the power passed through the window, and k is the thermal conductivity.

where $f(\rho)$ describes the shape of the incident beam and f_o is a beam-shape dependent normalization factor; note that the solution does not involve the heat-transfer coefficient or the window diameter. As demonstrated elsewhere [35], if the beam has a Gaussian shape, that is,

$$f(\rho) = \exp(-2W\rho^2) \ , \tag{47}$$

the solution can be approximated by means of a fourth-order even polynomial,

$$\delta T^*(\rho) \simeq \delta T_0^* - \delta T_2^* \rho^2 + \delta T_4^* \rho^4 \ , \tag{48}$$

which implies that the quartic term $\delta T_4^* \rho^4$ will be responsible for any beam-induced aberration. Consequently, since failure in the sense of Maréchal means a Strehl ratio of 0.8 or less [27], Eq. (29) indicates that the condition

$$\sqrt{\text{var}[OPD]} \leq \lambda/14 \tag{49}$$

must be satisfied, which tells us [see Eq. (45)] that the allowable power, or power that can be passed without degrading the target irradiance, is

$$P_{\text{lim}} = \frac{(\lambda/14)k}{\chi A_W} \cdot \frac{1}{\delta T_4^* \sqrt{\text{var}[\rho^4]}} \tag{50}$$

after refocusing.

Since the spherical aberration factor $S^* = \delta T_4^* \sqrt{\text{var}[\rho^4]}$ depends only on the truncation parameter W ($0.015 \leq S^* \leq 0.030$), it is then a simple matter to estimate the power-handling capability. In the near IR, the absorbance A_W of a defect-free diamond window should be dominated by AR-coating associated surface losses, which means $A_W \simeq 2 \times 10^{-3}$. On that basis, and upon inserting numbers as listed in Table 1, Eq. (50) in conjunction with the expression (44) for the optical distortion coefficient χ points to allowable average power levels in the 200 to 400 kW range. Operation at liquid nitrogen temperatures ($k \simeq 34$ Wcm^{-1}K^{-1}) may substantially enhance this performance, which far exceeds the power-handling capability of established laser-window materials but falls short of the "hundreds of megawatts" predicted by others [3]. In a CW mode of operation, the allowable beam intensity on axis derives immediately from the allowable beam power and should be of the order of 10 MW/cm^2 for a 1-cm diameter aperture, if the truncation parameter is indicative of very narrow beams ($W \simeq 10$). In the "micropulse" regime of free-electron lasers, the allowable peak intensity can be much larger because it relates to the average allowable intensity by way of the duty factor $DF = f\tau/N$, where f is the RF power frequency, τ is the pulse width, and N is the pulse spacing. For $f = 500$ MHz, $\tau = 50$ ps, and N as in Ref. 3, and on assuming that 10 MW/cm^2 is an applicable number for the time-averaged intensity, it is seen that, in principle, peak intensities of 4 GW/cm^2 could be passed without degrading the beam quality or creating laser damage [36].

4. Conclusion

The features that confer diamond its main advantage for optics applications in a thermally adverse environment are the thermal conductivity, which is much larger, and the thermal expansion, which is much smaller that those of other window/dome material candidates. Diamond has been promoted as the "ultimate" optical material, but there are limiting factors that must be taken into consideration. (a) Fairly substantial absorption occurs in the two- and the three-phonon bands, the peak absorption occurring at about 5 μm, which leads to the conclusion that diamond is not an acceptable missile-window material in the operationally desirable 3– to 5–μm spectral region. (b) The characteristic strength as well as the Weibull modulus of free-standing CVD diamond decrease as the thickness increases, which is indicative of a wide distribution of fracture probabilities at stress levels way below expectations that must be taken into account when CVD-diamond components are subjected to thermo-mechanical loads. (c) The oxidation rate of diamond becomes significant at temperatures above 600 °C, which implies that durable coatings will be required to provide adequate protection in a high-speed flight environment. Regarding potential applications as presently envisioned, our main conclusions are as follows.

- In the LWIR, aerodynamically heated missile domes do not degrade the system's performance even when the emittance exceeds 10 %, which translates into 8– to 12–μm absorption coefficients that are easily achievable with CVD diamond. As demonstrated in Fig. 2, diamond windows—flat plates as well as hemispherical shells—exhibit unmatched figures of merit for thermal shock, thus emphasizing the superior performance of this material in a thermally thin flight regime. In effect, at Mach 4 on a medium-altitude trajectory, the Biot number should be close to 0.002, which leads to an allowable heat flux about three hundred times larger that the heat load at the stagnation point of a 3–in diameter dome.

- Figure 4 displays the ranking of HEL mirror material candidates based on an index of merit as defined in Sec. 3.2. This procedure confirms that mirror faceplate materials can be ranked with regard to overall performance, that is, the performance in both applications, single pulse and steady state. It is seen that carbon/carbon and diamond are the outstanding candidates, diamond exhibiting particular promise for high-heat-load applications that require efficient cooling, which undoubtedly will attract increasing attention as CVD-diamond technologies mature.

- In the near IR, defect-free synthetic diamonds should have absorption coefficients as low as 1×10^{-4} cm^{-1}, which makes diamond an obvious candidate for high-power laser-window applications. Unfavorable refractive index characteristics, however, may result in thermal lensing at power levels substantially below initial expectations. Edge-cooled configurations cannot handle an average power of more than half a megawatt without inducing severe phase distortion, which means on-axis average beam intensities of up to 10 MW/cm^2 for a 1-cm diameter aperture in conjunction with very narrow beams typical of free-electron lasers.

Appendix: List of Symbols

a_∞ :	speed of sound	L :	window/dome thickness
A_M :	mirror absorbance	M_∞ :	Mach number
A_W :	window absorbance	n :	refractive index
Bi :	Biot number	p_∞ :	free-stream pressure
c :	velocity of light	P :	beam power
c_2 :	second radiation constant	Q :	heat flux
c_p :	specific heat of air	$Q(T)$:	quantum exitance function
$C_p^{'}$:	heat capacity	r :	radial coordinate
D :	aperture diameter	R :	dome radius
E :	Young's modulus	t :	elapsed time
$\overline{E}$:	average emittance	T_B :	background scene temperature
E' :	modified elastic modulus	T_D :	dome temperature
$f(\rho)$:	beam shape function	T_{iw} :	initial wall temperature
f_o :	normalization factor	T_{st} :	stagnation temperature
h :	heat-transfer coefficient	T_o :	room temperature
H_{eff} :	net effective irradiance	T_∞ :	free-stream temperature
I :	beam intensity	W :	truncation parameter
k :	thermal conductivity	z :	axial coordinate
l :	mirror faceplate thickness	Z_o :	target range

α :	thermal expansion coefficient	ν :	Poisson's ratio
γ :	specific heat ratio	ϕ :	background photon flux
ϵ_z :	axial strain	ρ :	reduced radial coordinate
δl :	thickness increment	ρ_∞ :	density of air
δT :	temperature increment	σ :	applied stress
$\delta\phi$:	phase aberration	σ_f :	flexural strength
Δp :	pressure differential	$\sigma_{\max}$:	maximum stress
ΔT :	temperature differential	σ_p :	peak stress
λ :	IR/laser wavelength	τ_o :	optical efficiency
μ_∞ :	viscosity of air	χ :	optical distortion coefficient

BPF :	beam profile factor	$(NEI)_o$:	dark-system NEI
DSF :	design safety factor	OPD :	optical path difference
FoM :	figure of merit	SNR :	signal-to-noise ratio
FSF :	fracture statistical factor	$(SNR)_o$:	dark-system SNR
GF :	Gaussian focus	SR :	Strehl ratio
NEI :	noise-equivalent irradiance	TSF :	thermal stress factor

References

1. R. Seitz, "The end of the beginning," *SPIE Proc.* **969**, 124 (1988).
2. C. Klein, T. Hartnett, and C. Robinson, "Critical-point phonon frequencies of diamond," *Phys. Rev. B* **45**, 12854 (1992).
3. S. Singer, "Diamond: A high-power optical material," *SPIE Proc.* **1275**, 2 (1990).
4. D. Gray, ed., *American Institute of Physics Handbook,* McGraw-Hill Book Co., New York (1972).
5. D. Harris, *Infrared Window and Dome Materials*, SPIE Press, Bellingham/WA (1992).
6. C. Klein and G. Cardinale, "Young's modulus and Poisson's ratio of CVD diamond," *Diamond and Rel. Mater.* **2**, 918 (1993).
7. C. Klein, R. Hallock, and R. Miller, "Chemically vapor-deposited diamond: Strains, stresses, and fracture strength," *ECS Proc.* **95-4**, 661 (1995).
8. M. Weber, ed., *CRC Handbook of Laser Science and Technology*, CRC Press, Boca Raton (1986).
9. J. Field, ed., *The Properties of Natural and Synthetic Diamond,* Academic Press, London (1992).
10. H. McSkimin and P. Andreatch, "Elastic moduli of diamond as a function of pressure and temperature," *J. Appl. Phys.* **43**, 3944 (1972).
11 C. Klein, T. Harnett, R. Miller, and C. Robinson, "Lattice vibrational modes and defect-activated IR absorptions in CVD diamond," *ECS Proc.* **91-8**, 435 (1991).
12. J. Rowe, A. Blume, and E. Boudreaux, "Dual-mode dome requirements for future air-to-air missiles," *Proc. Third DoD Symp. Electromagnetic Windows*, GACIAC/Chicago, vol. 1, p. 79 (1989).
13. C. Klein, "Hot infrared domes: A case study," *SPIE Proc.* **1326**, 217 (1990).
14. J. Hardy and S. Smith, "Two-phonon infrared lattice absorption in diamond," *Phil. Mag.* **6**, 1163 (1961).
15 M Thomas, W Tropf, and A. Szpak, "Optical properties of diamond," *Diamond Films and Tech.* **5**, 159 (1995)
16. S. Timoshenko and S. Krieger, *Theory of Plates and Shells*, McGraw-Hill Book Co., New York (1959).
17. C. Klein, "Infrared missile domes: Is there a figure of merit for thermal shock?," *SPIE Proc.* **1760**, 338 (1992).
18. D. Hasselman, "Thermal stress resistance parameters for brittle refractory ceramics· A compendium," *Ceram. Bull.* **49**, 1033 (1970).
19. C. Lee, "Evaluation of several IR/RF dome configurations subjected to high-speed flight environments," *Proc. Fourth DoD Symp. Electromagnetic Windows*, ONT/Arlington, vol. 1, p. 24 (1991).
20. C. Klein, "Thermal shock resistance of infrared missile domes: Analysis and testing," *Proc. Fifth DoD Symp. Electromagnetic Windows*, AFML/WPAFB, vol. 2, p. 3 (1993).
21. A. Shapiro, *The Dynamics and Thermodynamics of Compressible Fluid Flow*, The Ronald Press, New York (1953).

22. C. Klein, "Infrared missile domes: Heat flux and thermal shock," *SPIE Proc.* **1997**, 150 (1993).
23. F. Schmid, C. Khattak, and D. Felt, "Sapphire sparkles in many optical elements," *Laser Focus/World* **32-6**, 167 (1996).
24. T Zien and W. Ragsdale, "Predictions of aerodynamic heating on tactical missile domes," *NTIS Document No.* **NSWC-TR-79-21** (1979).
25. B. Bendow and P. Giannino, "Optics of thermal lensing in solids," *Appl. Opt.* **12**, 710 (1973).
26 C. Klein, "Thermally induced optical distortion in high-energy laser systems," *Opt. Eng.* **18**, 591 (1979).
27. M. Born and E. Wolf, *Principles of Optics*, Pergamon Press, Oxford (1975).
28. D. Holmes and P. Avizonis, "Approximate optical system model," *Appl. Opt.* **15**, 1075 (1975).
29. B. Boley and J. Weiner, *Theory of Thermal Stresses*, J. Wiley & Sons, New York (1960).
30. F. Anthony, "High-heat-load optics: An historical overview," *Opt. Eng.* **34**, 313 (1995).
31. C. Klein, "Mirror figure of merit and material index of goodness for high-power laser beam reflectors," *SPIE Proc.* **288**, 69 (1981).
32. C. Pellerin, F. Ayer, Y. Mehrotra, and A. Hopkins, "New opportunities from materials selection trade-offs for high-precision space mirrors," *SPIE Proc.* **542**, 5 (1985).
33. D. Hamilton, E. Hoag, and J. Seitz, "Diamond as a high-power laser window," *J. Opt. Soc. Am.* **64**, 36 (1974).
34. M. Sparks, "Optical distortion by heated windows in high-power laser systems," *J. Appl Phys.* **42**, 5029 (1971).
35. C. Klein, "High-power CW laser windows: Edge cooled or face cooled?," *SPIE Proc.* **1739**, 230 (1992).
36 C. Klein and R. DeSalvo, "Thresholds for dielectric breakdown in laser-irradiated diamond," *Appl. Phys. Lett.* **63**, 1895 (1993).